The Meteoritical Society

Meteoritics & Planetary Science 43, Nr 1/2, 233–246 (2008)
Abstract available online at http://meteoritics.org

TOF-SIMS analysis of cometary matter in Stardust aerogel tracks

Thomas STEPHAN[1†*], Detlef ROST[2], Edward P. VICENZI[2], Emma S. BULLOCK[2], Glenn J. MACPHERSON[2], Andrew J. WESTPHAL[3], Christopher J. SNEAD[3], George J. FLYNN[4], Scott A. SANDFORD[5], and Michael E. ZOLENSKY[6]

[1]Institut für Planetologie, Westfälische Wilhelms-Universität Münster, Wilhelm-Klemm-Str. 10, 48149 Münster, Germany
[2]Department of Mineral Sciences, National Museum of Natural History, Smithsonian Institution, Washington, DC 20560, USA
[3]Space Sciences Laboratory, University of California at Berkeley, Berkeley, California 94720, USA
[4]Department of Physics, SUNY Plattsburgh, Plattsburgh, New York 12901, USA
[5]Astrophysics Branch, NASA Ames Research Center, Moffett Field, California 94035, USA
[6]Astromaterials Research and Exploration Science, NASA Johnson Space Center, Houston, Texas 77058, USA
[†]Present address: Department of the Geophysical Sciences, University of Chicago, 5734 South Ellis Avenue, Chicago, Illinois 60637, USA
[*]Corresponding author. E-mail: tstephan@uchicago.edu

(Submitted 05 December 2006; revision accepted 08 April 2007)

Abstract–Cometary matter in aerogel samples from the Stardust mission was investigated with TOF-SIMS for its elemental and organic composition. While single grains >1 μm are highly variable in their chemical composition, nanometer-scale material found in the wall of one track has within a factor of 1.22 bulk CI chondritic element ratios relative to Fe for Na, Mg, Al, Ti, Cr, Mn, and Co. Compared to CI, a depletion in Ca by a factor of four and an enrichment in Ni by a factor of two was observed. These results seem to confirm recent reports of a CI-like bulk composition of Wild 2. The analysis of organic compounds in aerogel samples is complicated by the presence of contaminants in the capture medium. However, polycyclic aromatic hydrocarbons that could possibly be attributed to the comet were observed.

INTRODUCTION

The Stardust sample return mission collected cometary matter during the passage through the coma of comet 81P/Wild 2 in January 2004 (Brownlee et al. 2003, 2006; Tsou et al. 2003). Before the cometary encounter, during the cruise phase, Stardust also collected a sample of contemporary interstellar dust. The primary capture medium for both cometary and interstellar dust was low-density silica aerogel, with a total surface area of 1039 cm^2 exposed to the comet.

In order to determine its elemental, isotopic, mineralogical, and organic properties, the cometary matter captured by the aerogel collectors has to be either separated from the aerogel or analyzed in situ. Although removal of samples from the aerogel is preferred, since it facilitates detailed studies of the cometary material under more controlled conditions and enables a wider range of instrumental techniques to be employed, it is practically impossible in cases where an impacting cometary dust grain has disintegrated along the track. In these cases, in-situ analysis of the finely disseminated material is needed to determine the composition of the impactor.

In previous studies (Stephan et al. 2006a, 2006b), it was demonstrated that residual material in experimentally produced particle tracks in aerogel can be analyzed by time-of-flight secondary ion mass spectrometry (TOF-SIMS). In the present study, three aerogel samples from the cometary Stardust collection were analyzed with TOF-SIMS.

Some of the results reported here were already briefly mentioned in two publications by the Stardust Preliminary Examination Team (Flynn et al. 2006; Sandford et al. 2006).

SAMPLES AND EXPERIMENTAL TECHNIQUES

Sample Preparation

Dissected aerogel keystones were prepared following previously described routines (Westphal et al. 2004) from two tracks, Track 57 from Stardust aerogel cell C2009 and Track 21 from cell C2115.

A keystone fragment from Track 57 (C2009,13,57,0), hereafter T57, was investigated in this study. The keystone shown in Fig. 1 was dissected by placing an aerogel flight

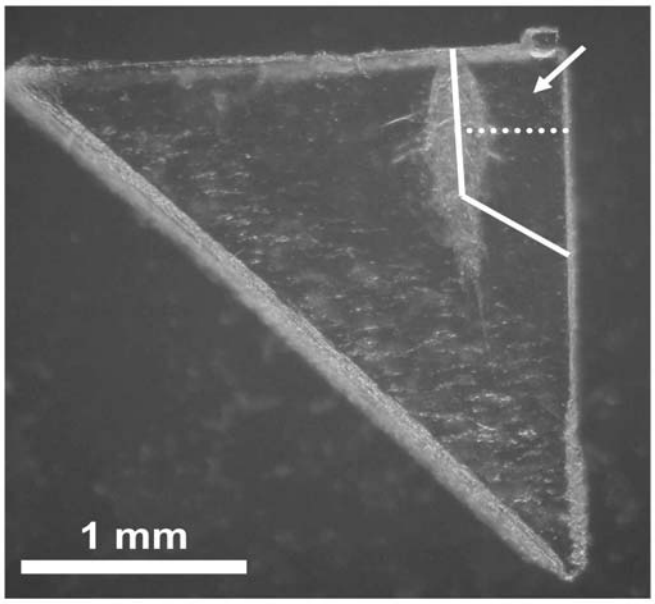

Fig. 1. An optical image of the Track 57 aerogel keystone from cell C2009. The keystone was dissected along the solid lines and broke afterwards along the dotted line. For this study, a fragment (T57) from the upper right in the image (arrow) was selected.

spare tile on its side. Then, using an automated "keystoning" system with a vertical glass needle, vertical cuts were made as shown in Fig. 1. The resulting aerogel piece was very fragile due to incipient radial cracks, visible in Fig. 1, resulting from the impact itself. In the process of handling, the aerogel piece broke into four fragments, along the dotted line in Fig. 1, and, in the other direction, looking straight down the particle trajectory, the track split in half. For this study, one of the fragments that included the mouth of the track was selected.

In the case of Track 21, two samples were prepared from one keystone as outlined in Fig. 2. First, the bulb of the track was dissected lengthwise. Then six slices, each ~100 μm thick, were cut at a 45° angle. From these diagonal slices, two were selected for TOF-SIMS analysis, slice #2 (C2115,30,21,0), hereafter T21-2, and slice #6 (C2115,34,21,0), hereafter T21-6.

All three aerogel samples were flattened after dissection, since TOF-SIMS ideally requires flat surfaces. Flattening was achieved by pressing each aerogel slice between a 5 × 5 mm^2 silicon chip and a glass slide, using a microscope as a press as described by Stephan et al. (2006a). After flattening, the samples were flat to within a few micrometers and adhered reliably to the silicon chip, with the track material exposed uppermost. Figure 3 shows an optical microscope image of sample T57 after flattening.

Samples T57 and T21-6 were sent to the Institute for Planetology at Münster University and T21-2 was sent to the National Museum of Natural History at the Smithsonian Institution in Washington, D.C., for TOF-SIMS analysis and variable pressure scanning electron microscopy (VP SEM) imaging. Both laboratories are equipped with TOF-SIMS IV instruments from ION-TOF GmbH.

TOF-SIMS Technique

TOF-SIMS has several advantages over most other analytical techniques for in-situ analysis of Stardust samples in aerogel, as described by Stephan et al. (2006a). In particular, TOF-SIMS works well on insulating materials like aerogel and eliminates the need for applying a conductive coating to the sample.

In the present study, all analyzed surfaces had to be cleaned by Ar^+ ion sputtering prior to the actual analysis. Although sputtering is known to destroy organic molecules by fragmentation, cleaning was mandatory since all aerogel surfaces showed an omnipresent contamination layer preventing any SIMS analysis of the cometary material. For analysis, an intermittent Ga^+ primary ion beam with a pulse length of 1.5 ns was used. With repetition rates of 10,000 (Münster) and 22,222 (Washington) shots per second, the analyzed sample regions were raster-scanned with 128^2 or 256^2 pixels and 8–128 shots per pixel in each scan. Each measurement consists of 50–12,000 scans. Combinations of these parameters were selected to allow total measurement times of 6–25 h. Each stack of images was corrected for sample shift before being added together. Further details on the TOF-SIMS technique are given by Stephan (2001).

All quantitative elemental results in this study are given as atomic element ratios relative to Fe. Iron was chosen as the reference element, since the aerogel capture material is essentially SiO_2, and therefore Si is not a suitable reference element. Magnesium as reference element would be another possible choice, because it is also a major element in the cometary dust. However, Fe was selected since it can also be used as reference element for Fe,Ni sulfides that are also frequently found in Wild 2 samples. Relative sensitivity factors obtained from glass standards that are usually used for quantitative TOF-SIMS analysis of silicates (Stephan 2001) were applied. The uncertainty for such an approach is expected to be of the order of a factor of <1.5. Even for non-silicate particles, the derived metal-to-iron ratios should be of comparable accuracy.

Variable Pressure SEM

Low energy secondary electron (SE) imaging and VP SEM was performed on slice T21-2 using an FEI Nova NanoSEM 600, which employs a field emission electron source. Because silica aerogel is a strong electrical insulator, one would typically be faced with either applying a thin coating of a conductive film (e.g., carbon), or using a low energy electron beam. In this study, however, yet another method was used in addition to low-energy SE imaging: A small partial pressure of water vapor (~0.5 hPa) was

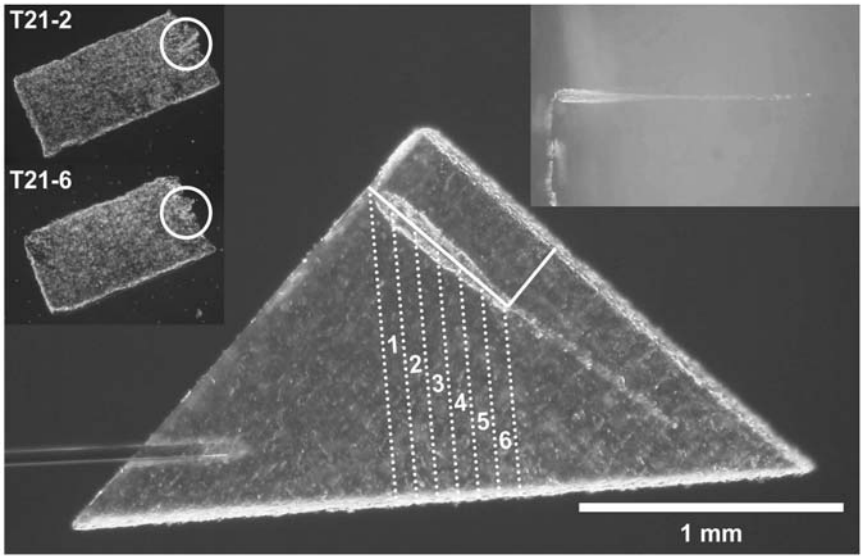

Fig. 2. An optical image of the Track 21 aerogel keystone from cell C2115. The track, still sitting in the aerogel cell before keystone extraction, is shown from another angle in the upper right. After preparation of the keystone, the bulb of the track was dissected lengthwise (solid line). Then, six slices were cut at 45° angle (dotted lines). Slices #2 and #6 (upper left) were analyzed with TOF-SIMS. The position of the track is indicated by circles.

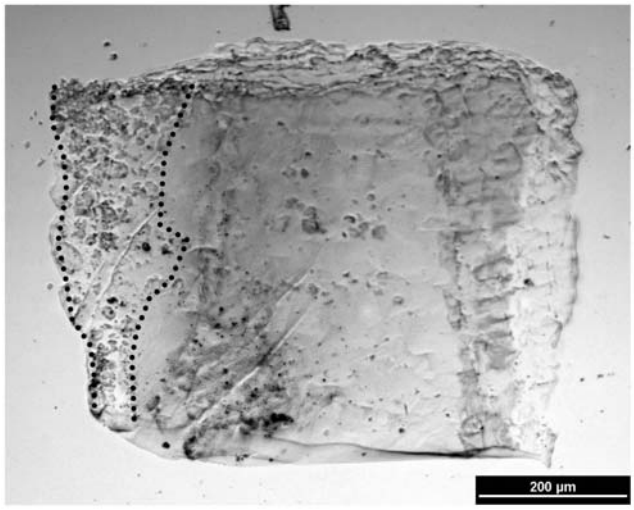

Fig. 3. Reflected light microscope image of sample T57 after flattening. The bulbous part of the dissected aerogel track is outlined by dotted lines.

introduced during imaging to create positively charged H_2O ions that acted to neutralize the excess negative charge from the electron beam. Such charge neutralization allowed the use of sufficiently high beam energies to employ energy dispersive X-ray analysis on the aerogel.

Blank Correction

From its chemical properties, Stardust aerogel is nearly pure silica. However, it is contaminated with traces of elements other than Si and O. Since the cometary matter analyzed in this study could not be separated completely from the aerogel, correction for an aerogel blank had to be performed. Therefore, the composition of the aerogel close to the investigated tracks was also determined. Apart from C, which is known to be present in the aerogel up to a few wt% (Sandford et al. 2006) and is difficult to quantify by TOF-SIMS, atomic element ratios relative to Si = 10^6 for all trace elements detected by TOF-SIMS are given in Table 1. Here, for quantification, the same relative sensitivity factors from glass standards were used as described above.

Both elements that are suitable as reference elements for TOF-SIMS quantification, Fe and Mg, are not significant contaminants in the aerogel if compared with cometary matter, where these elements are expected to be major components. This is especially true for Fe that is also a major element in Fe sulfides and has therefore been selected as the reference element throughout this study.

However, for a mathematically correct blank correction, one has to consider that for each element *E*, an aerogel blank has to be subtracted:

$$E_r = E - E_b, \tag{1}$$

where element designations without indices describe secondary ion signals measured by TOF-SIMS, those with index *r* denoting the cometary residue, and those with index *b* standing for the aerogel blank.

For the sought-after element-to-iron ion ratios in the cometary residues follows

$$\left(\frac{E}{Fe}\right)_r = \frac{E}{Fe_r} - \frac{E_b}{Fe_r}. \tag{2}$$

This can easily be transformed to

$$\left(\frac{E}{Fe}\right)_r = \frac{E}{Fe}\frac{Fe}{Fe_r} - \left(\frac{E}{Fe}\right)_b\left(\frac{Fe}{Fe_r} - 1\right). \quad (3)$$

Here, the only ratio that could not be measured directly is Fe/Fe_r that, however, is expected to be close to unity, because the majority of detected Fe ions should come from the cometary residue.

The actual Fe/Fe_r ratio can be traced back to known quantities and the Si/Fe ion ratio of the cometary matter $(Si/Fe)_r$:

$$\frac{Fe}{Fe_r} = \frac{(Si/Fe)_r - (Si/Fe)_b}{Si/Fe - (Si/Fe)_b}. \quad (4)$$

The $(Si/Fe)_r$ ratio has to account for the expected but indistinguishable cometary Si in the residue. In the present study, a CI chondritic Si/Fe ratio in the cometary matter has been assumed. This neither implies that Wild 2 dust is expected to be mineralogically similar to CI chondrites, nor does this introduce a preconception regarding other element ratios. CI chondritic abundances are used as an approximation for solar system abundances (Anders and Grevesse 1989).

In some cases, where samples were found to be rather Fe-poor but Mg-rich or where Fe seems to be present in a sulfide that is not expected to contain any Si, a CI-like Si/Mg ratio was assumed to estimate the cometary Si. Certainly, the use of CI chondritic Si/Fe or Si/Mg ratios is only a first-order approximation. However, for all investigated sample areas and all particles, it is estimated that >96.7% of the Si comes from aerogel. Therefore, an uncertainty in the indigenous Si content has only a minor effect on the determined element ratios, smaller than the statistical errors. Even if the Si content of the sample were by a factor of two higher than estimated, the blank subtraction would only be affected by <3.5%. It makes little practical difference exactly what cometary Si is assumed, because Si is so dominated by the aerogel signal that these differences make only tiny modifications to the blank correction.

Finally, all data were discarded wherever the blank was found to be higher than 50% of the entire signal or where the lateral distribution of the contamination was clearly heterogeneous, and therefore the measured signal could not be unambiguously attributed to cometary material.

It should be noted that the mathematical details of the blank correction are identical to the procedures described by Leitner et al. (2008) for the blank correction of impact residues on Stardust Al foil. To illustrate the effect of blank correction in the present study, detailed secondary ion data for all measurements are tabulated in the Appendix.

Organics

One goal of the investigation of Stardust aerogel samples was the analysis of cometary organics. Analyzing these samples directly in the aerogel minimizes the risk of contamination. On the other hand, the possibility that aerogel may act like a sponge for volatile organic compounds and that contamination may have occurred at various stages prior to the sample preparation cannot be excluded. To test for possible contamination, a tile of aerogel was mounted on the collector tray deployment arm (Sandford et al. 2006). This Flight Aerogel Witness Tile was placed so that it was protected from impacts during the Wild 2 flyby by the spacecraft's dust shields. Thus, this tile witnessed all the same environments (terrestrial and space) as the cometary collector tiles, but was not exposed to the comet. It therefore represents an ideal control sample for the study of cometary organics in aerogel, and a piece from it (WCARMI1CPN,12) was also investigated by TOF-SIMS. This analysis was performed without prior Ar^+ sputtering to ensure that no contamination was removed from

Table 1. Atomic element ratios relative to Si = 10^6 for aerogel blanks[a] from areas close to the investigated cometary matter.

Element	T57	T21-2	T21-6
Li	0.09 ± 0.09	0.93 ± 0.08	1.3 ± 0.5
B	19 ± 6	1410 ± 10	940 ± 60
Na	166 ± 3	212 ± 1	217 ± 5
Mg	2.6 ± 0.7	25.1 ± 0.6	33 ± 4
Al	8 ± 2	2.9 ± 0.2	5 ± 3
K	55 ± 1	123 ± 1	84 ± 2
Ca	0.2 ± 0.3	0.9 ± 0.1	6 ± 1
Sc	0 ± 1		3 ± 2
Ti	0.9 ± 0.9	2.7 ± 0.3	5 ± 2
V	2 ± 1		
Cr		1.3 ± 0.2	1 ± 2
Mn	3 ± 4	0.6 ± 0.1	2 ± 7
Fe	26 ± 4	31 ± 2	80 ± 20
Co		0.1 ± 0.2	
Ni	0 ± 5	5 ± 1	
Cu	21 ± 7		

[a]Uncertainties are given as 1σ statistical errors that do not reflect uncertainties from the relative sensitivity factors.

Table 2. Atomic element ratios relative to Fe and corrected for aerogel blank for 3 particles found in T57.[a]

Element	Particle #1	Particle #2	Particle #3
Li	0.017 ± 0.002		0.010 ± 0.003
B	1.44 ± 0.09		
Na	187.0 ± 0.2	0.0267 ± 0.0003	5.68 ± 0.05
Mg	54.9 ± 0.2	0.0042 ± 0.0002	8.7 ± 0.1
Al	64.4 ± 0.3		1.09 ± 0.04
K	85.6 ± 0.1	0.00255 ± 0.00008	0.262 ± 0.009
Ca	26.1 ± 0.1	0.00015 ± 0.00003	0.75 ± 0.02
Ti	0.65 ± 0.08		0.06 ± 0.01
Cr	0.029 ± 0.004		0.23 ± 0.02
Mn			0.05 ± 0.01
Fe	1.00 ± 0.05	1.000 ± 0.008	1.00 ± 0.08
Ni	0.04 ± 0.03	0.004 ± 0.001	0.06 ± 0.03
Ba	0.055 ± 0.004		

[a]Uncertainties are given as 1σ statistical errors that include statistical errors from the blank correction but do not reflect uncertainties from the relative sensitivity factors.

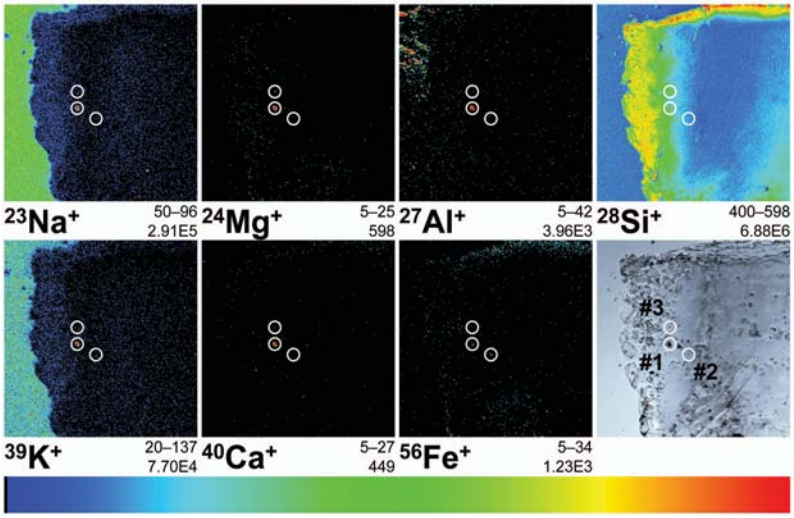

Fig. 4. Secondary ion images of a region (500 × 500 μm^2) on flattened silica aerogel fragment T57. The area was raster-scanned with 256 × 256 pixels and 128 shots per pixel in each of 50 scans (a total of 6400 shots/pixel). All individual ion images here and in subsequent figures use the same linear color scale shown, where black corresponds to zero counts and red is used for the maximum intensity or an intensity range given below every image (e.g., 50–96 counts for $^{23}Na^+$). The other number underneath each image is the integrated intensity of the entire field of view (e.g., 2.91 × 10^5 counts for $^{23}Na^+$). The outline of the track is scarcely visible in the ion images. However, three minor particles (#1, #2, and #3) were identified in several ion images and selected for detailed analysis (Fig. 5).

the control sample and no large molecules were fragmented. Therefore, the amount of organic compounds observed on the control sample represents only an upper limit for the contamination expected to be found after sputtering on aerogel exposed to the comet. Any surplus in the latter samples can be attributed to the comet.

RESULTS AND DISCUSSION

T57

The results of a TOF-SIMS imaging survey of sample T57 are shown in Fig. 4. No fine-grained material is visible along the track in the secondary ion images, and only three minor particles are observed in some of these images. It is not surprising that these particles are found "outside" the obvious track, since a lot of cracks extend into the aerogel volume from Track 57 as can be seen in Fig. 1, and the aerogel naturally fractures along pre-existing cracks.

The three particles were further analyzed by TOF-SIMS at higher magnifications. The imaging results are shown in Fig. 5, and quantitative results are summarized in Table 2.

Particle #1, 12 μm × 7 μm in size, contains abundant F, Na, Mg, Al, Cl, K, and Ca (Fig. 5 #1; Table 2). A proper quantification, however, is not possible for F and Cl because of a lack of appropriate standards for these elements. Li, B, Ti, Cr, Fe, Ni, and Rb are found at much lower concentrations. An extremely high ratio for Si/Fe (~5300) can be attributed to aerogel intimately intermingled with the particle. In fact, the observed particle is dominated by aerogel. Since the absolute Si abundance of the cometary portion of this particle cannot be determined, a mineralogical discrimination is not possible. Another puzzling characteristic of this particle, however, is the presence of H- and C-bearing compounds on its surface, as can be seen in the H^-, C^-, CH^-, OH^-, and CN^- images (Fig. 5 #1), that were not completely removed by Ar^+ sputtering and appear in a ring structure.

Particle #2, 3 μm × 2 μm in size, is less dominated by aerogel than Particle #1 as shown in Fig. 5 (#2). A Si/Fe ratio of ~3 was observed for this particle. High levels of Fe and S and trace abundances of Na, Mg, K, Ca, and Ni were detected (Fig. 5 #2 and Table 2). Besides aerogel, this particle is predominately an iron sulfide with a low Ni content.

Particle #3, 3 μm × 1.5 μm in size, is rich in Na and Mg. Minor or trace elements are Li, Al, K, Ca, Ti, Cr, Mn, Fe, and Ni (Fig. 5 #3). The Si/Fe ratio is ~240, much higher than for Particle #2, but clearly below the extraordinarily high ratio of Particle #1. Nonetheless, the composition of this particle is strongly overprinted by aerogel.

None of the three particles is chondritic in composition. However, particles #1 and #3 both have chondritic Fe/Ni ratios within the limits of uncertainty, and low-Ni iron sulfides such as particle #2 were found in several Wild 2 samples (Zolensky et al. 2006). It therefore seems likely that all three particles represent actual cometary material.

T21-2 and T21-6

Figure 6 shows optical microscope images of both samples from C2115 investigated in this study. Each sample contains a portion of Track 21 at one of its edges. Figure 7 shows secondary ion overview images for T21-2 and T21-6,

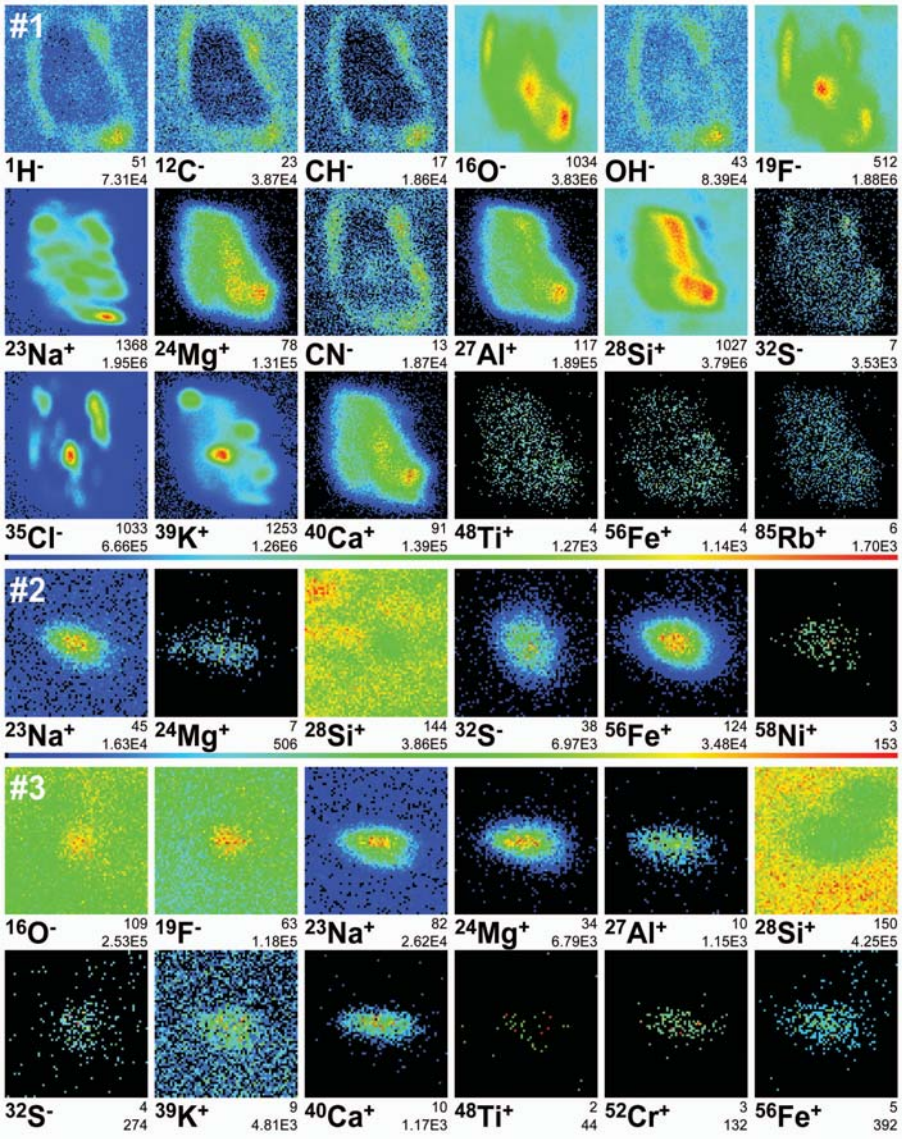

Fig. 5. Detailed secondary ion images of three particles (#1, #2, and #3) from sample T57. The locations of the particles in the original track are shown in Fig. 4. Fields of view are 12 × 12 μm^2 (98 × 98 pixels, 12,800 shots/pixel) for particle #1 and 5 × 5 μm^2 (65 × 65 pixels, 6400 shots/pixel) for particles #2 and #3.

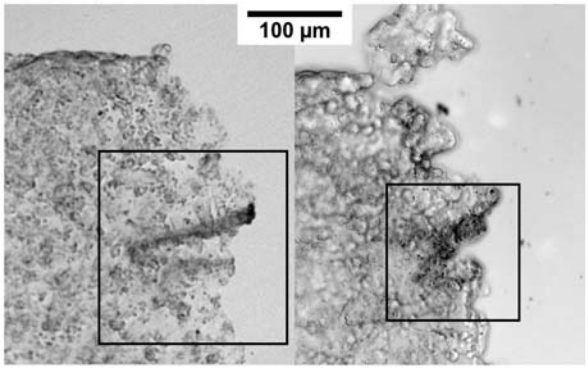

Fig. 6. Reflected light optical microscope images of samples T21-2 (left) and T21-6 (right). The marked areas were investigated using TOF-SIMS (Fig. 7).

respectively. In both cases, the sections of the particle track can be seen in the Mg, Al, and Fe secondary ion images as cometary material implanted into the wall of the track bulb.

A low energy SE image of T21-2 is given in Fig. 8, showing two selected smaller regions that were subsequently analyzed by TOF-SIMS. The secondary ion images from these two analyses are shown in Fig. 9.

Element ratios for all four measurements (two overview and two detailed) of cometary material in the track sections were determined. This was achieved by summing areas of high contrast in secondary ion images. These regions of interest comprise the dominant chemical signature (e.g., Mg, Al, and Fe) of the cometary impactor. This spatial summation approach reduces the influence of aerogel contamination. A blank correction was then applied as described above. The

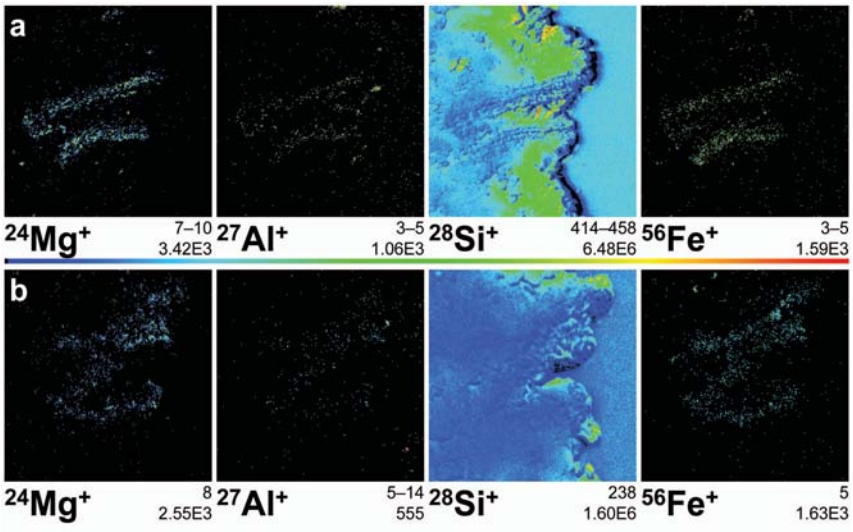

Fig. 7. TOF-SIMS secondary ion images from (a) a region 200 × 200 μm² in size from sample T21-2 (253 × 253 pixels, 17,280 shots/pixel) and (b) a region 140 × 140 μm² in size from sample T21-6 (239 × 239 pixels, 6400 shots/pixel).

Table 3. Atomic element ratios relative to Fe and corrected for aerogel blank[a] for all sample areas from Track 21. Geometric mean values[b] are given as best estimates for the track composition.

Element	T21-6	T21-2	Detail #1	Detail #2	Geometric mean
Na	0.080 ± 0.004			0.0456 ± 0.0007	0.06 ± 0.02
Mg	0.63 ± 0.01	1.04 ± 0.02	1.651 ± 0.007	1.387 ± 0.005	1.1 ± 0.4
Al	0.065 ± 0.004	0.120 ± 0.007	0.120 ± 0.002	0.082 ± 0.003	0.09 ± 0.02
Ca	0.014 ± 0.002	0.013 ± 0.002	0.0194 ± 0.0009	0.0315 ± 0.0007	0.018 ± 0.007
Ti		0.004 ± 0.002	0.0025 ± 0.0004	0.0012 ± 0.0003	0.0024 ± 0.0012
Cr	0.013 ± 0.003	0.014 ± 0.003	0.0141 ± 0.0008	0.0175 ± 0.0007	0.015 ± 0.002
Mn	0.009 ± 0.005	0.010 ± 0.004	0.019 ± 0.001	0.0128 ± 0.0009	0.012 ± 0.004
Fe	1.00 ± 0.03	1.00 ± 0.04	1.00 ± 0.02	1.00 ± 0.01	≡1
Co	0.005 ± 0.003	0.003 ± 0.002	0.0029 ± 0.0006	0.0022 ± 0.0004	0.0030 ± 0.0010
Ni	0.14 ± 0.02	0.19 ± 0.02	0.067 ± 0.007	0.095 ± 0.007	0.11 ± 0.05

[a]Uncertainties are given as 1σ statistical errors that include statistical errors from the blank correction but do not reflect uncertainties from the relative sensitivity factors.
[b]Geometric mean values were calculated from the four different measurements.

Table 4. Correlation coefficients (CC) between element ratios from Track 21 (geometric mean values) and those from chondrite types (Lodders and Fegley 1998)

Chondrite type	CC	Chondrite type	CC
CI	0.996	H	0.998
CM	0.995	L	0.979
CV	0.987	LL	0.965
CO	0.992	R	0.997
CK	0.984	Acapulcoites	0.983
CR	0.993	K	0.988
CH	0.962	EH	0.983
		EL	0.995

resulting element ratios relative to Fe and normalized to CI chondritic abundances are shown in Fig. 10, while the unnormalized element ratios are given in Table 3. Geometric mean values are given as best estimates for the track composition.

It is important to note that metals, usually considered major elements, are found in these samples as trace elements. For example, Fe and Mg together have concentrations of less than 1% by weight, with silica comprising the balance (~99%). The quantitative results reveal that the analyzed cometary material has CI chondritic composition within a factor of 1.22, except for a significant depletion in Ca (factor of four), and to a lesser extent, an enrichment in Ni (factor of two).

To evaluate this resemblance with CI, the measured element ratios were compared with element ratios of different chondrite classes (Lodders and Fegley 1998). Correlation coefficients were calculated between TOF-SIMS data and all chondrite classes (Table 4). Among carbonaceous chondrites, the highest correlation coefficients of 0.996 and 0.995 were found for CI and CM chondrites, respectively. However, also for H, R, and EH chondrites correlation coefficients of 0.995–0.998 were calculated. None of the chondrite classes yield a correlation

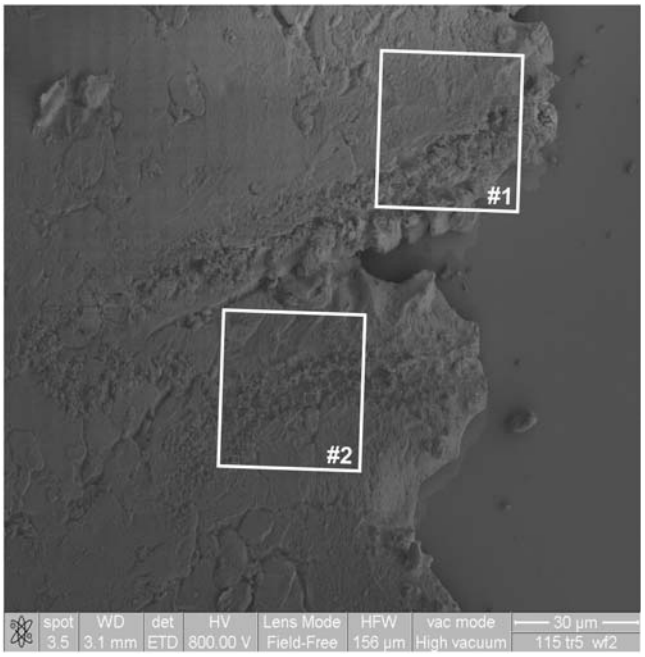

Fig. 8. Low energy (800 eV) SE image of sample T21-2. The entire area shown was analyzed by TOF-SIMS (Fig. 7a), while the white squares represent regions of subsequent analyses (Fig. 9).

coefficient below 0.96. These results show that from the available data set in this study, an unequivocal assignment to a specific chondrite class could not be made. For better classification, data for light elements, especially C, would be crucial. However, the data clearly prove the chondritic nature of Wild 2 matter and is consistent with CI or solar system abundances.

The Fe distribution along Track 21 was mapped in a previous study using synchrotron-based X-ray microprobe (SXRM) analysis (Flynn et al. 2006). Less than 10% of the total Fe mass was found in the terminal particle, indicating that most of the material of the initial particle was deposited in the bulb. Assuming that the material is distributed homogeneously throughout the bulb wall, it can be estimated that <40 pg of cometary material resides in each of the two aerogel slices investigated by TOF-SIMS.

The good agreement with the CI chondritic composition found in the present study exemplifies that although only a tiny fraction of the particle originally impacting the aerogel tile was analyzed in these measurements, this track wall material seemingly provides a reasonable approximation of the original grain's composition or at least of a major, rather chondritic portion of the original particle.

Discerning the precise dimensions of the diffuse cometary material in flattened aerogel slices is non-trivial. Following TOF-SIMS data collection, higher magnification imaging using VP SEM was performed on slice T21-2 in an effort to correlate microstructural features with the contrast in the secondary ion images (Fig. 9). However, no micrometer- to sub-micrometer-sized features could be unambiguously recognized in the electron imagery (Fig. 11). Additionally, X-ray spectrum imaging of this sample revealed no contrast in Mg, Al, Ca, and Fe element maps. Therefore, the maximum size of cometary grains in the analyzed aerogel must be well below 100 nm.

A possible scenario would be that the impacting cometary particle consisted of extremely fine-grained minerals together with some coarser grains that probably consist of many smaller grains themselves. These minerals might altogether have been embedded in an icy matrix. During aerogel impact, the ice vaporized explosively, distributing ultrafine material in the walls of the emerging bulbous part of the track. Some coarser grains, less affected by the explosive vaporization, continued their path through the aerogel and were found as terminal particles or larger fragments.

The multitude of secondary ion features showing a collective CI chondritic composition differs markedly from the three isolated particles from T57 that have non-chondritic compositions. Large particles that are dominated by a single or by just a few minerals are not expected to show chondritic composition since no single mineral exists that has a chondritic element pattern. Fine-grained material, analogous to matrix material in chondritic meteorites, may consist of a multitude of minerals that in fact show CI-like abundances.

It is noteworthy and perhaps surprising that results from such a tiny fraction of one single particle track in aerogel yields major element abundances close to the overall abundance of comet Wild 2 as deduced from a multitude of samples from various sample types (Flynn et al. 2006).

The observed abundance pattern (CI chondritic composition with a significant depletion in Ca) resembles the element composition observed for chondritic interplanetary dust particles (IDPs) collected in the stratosphere (Schramm et al. 1989; Arndt et al. 1996). The lack of Ca in IDPs is often attributed to the tendency of Ca to be present in larger minerals that are underrepresented in the chondritic IDP collection. Calcium was found in coarse-grained IDPs and some stratospheric particles that were probably miss-classified as being terrestrial due to their non-chondritic elemental composition. The same phenomenon may be responsible for the apparent Ca depletion in the fine-grained track material investigated in this study. Calcium-, Al-rich minerals found in some Wild 2 samples (Zolensky et al. 2006; Stephan et al. 2008) may account for the missing Ca.

Organics

As described above, the identification of cometary organics is challenged by the presence of organic contamination. However, polycyclic aromatic hydrocarbons (PAHs) were found in aerogel sample T21-6. The relative abundances of various PAH secondary ions depending on their number of C atoms are shown in Fig. 12. A clear association with the track material was not found. In contrast, deeper in the aerogel, in the region that was used to analyze

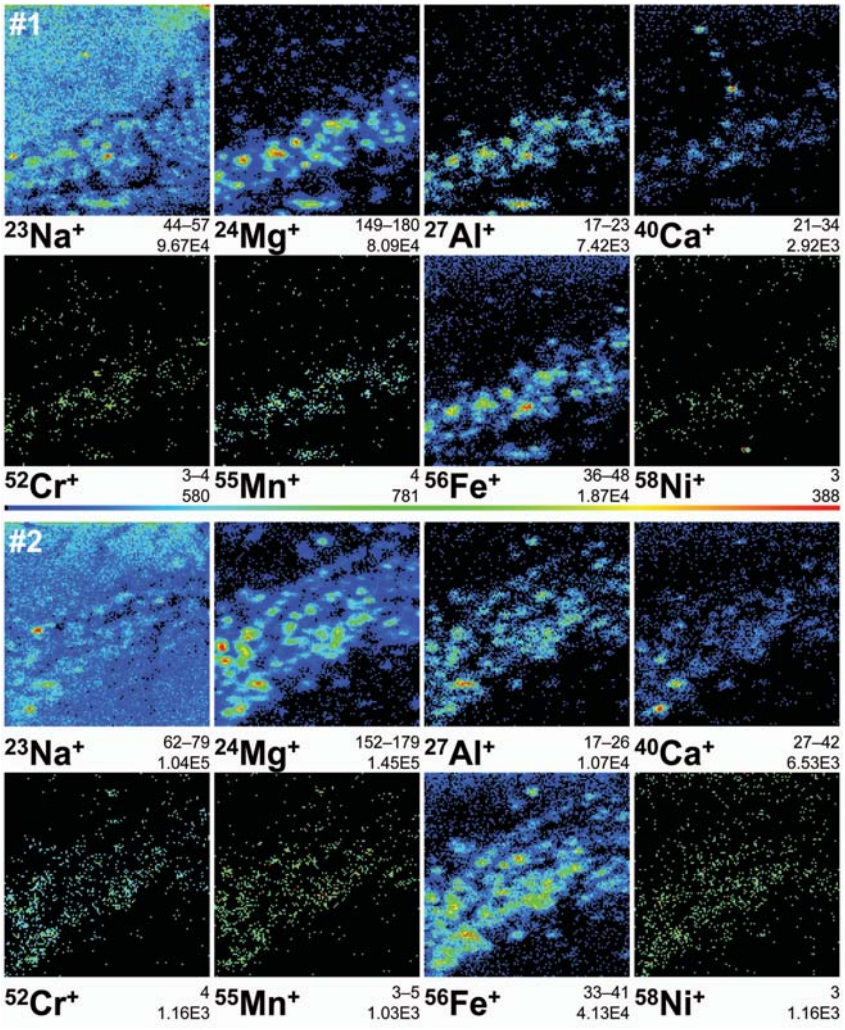

Fig. 9. Detailed secondary ion images of two regions (#1 and #2) from Fig. 8. Fields of view are 35 × 35 μm^2 (123 × 124 and 124 × 121 pixels, respectively, 96,000 shots/pixel) for both regions.

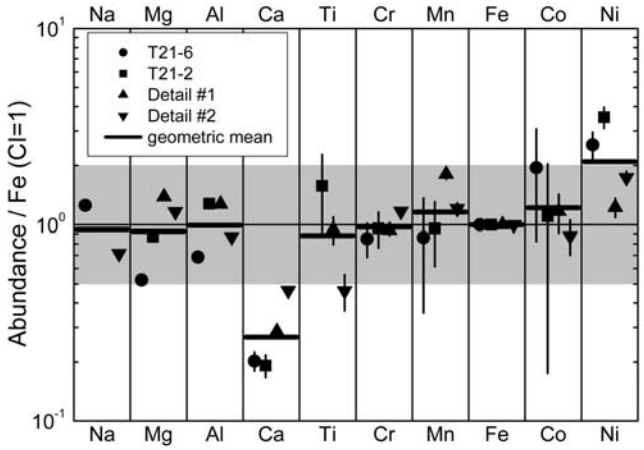

Fig. 10. Element ratios relative to Fe and normalized to CI chondritic abundances for both track regions shown in Fig. 7, as well as from two selected detail regions shown in Figs. 8 and 9. Most data points are within a factor of two (grey area) of chondritic ratios. Geometric mean values are within a factor of 1.22 chondritic except for Ca and Ni).

the element concentrations of the aerogel blank, PAH concentrations are even higher than in the actual track region. This might be explained by migration of PAHs deeper into the aerogel after their implantation. Injection of organics into the aerogel surrounding the tracks, which presumably occurred during impact, has also been seen in Stardust samples using infrared spectroscopy (Sandford et al. 2006; Bajt et al., Forthcoming). The apparent lower concentration in the actual track region compared to the surrounding aerogel might be explained by differences in secondary ion formation efficiencies for PAHs from disturbed (compacted and maybe partially molten) versus undisturbed aerogel.

Compared to the Flight Aerogel Witness Tile, which was not exposed to the comet, PAH concentrations are up to a factor of six higher in aerogel sample T21-6, although the unavoidable sputter cleaning should have diminished the PAHs in T21-6 (see above). It therefore seems likely that a major fraction of these PAHs in fact represent cometary organics.

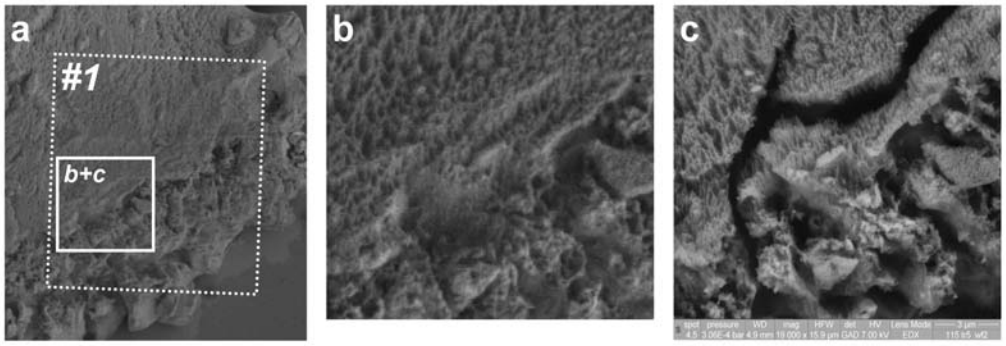

Fig. 11. SEM images of sample T21-2. a) This low energy SE overview image has a field of view of 50 × 50 μm^2 and indicates the region #1 of the preceding TOF-SIMS analysis (Fig. 9) and a box marking higher magnification SEM images in (b) and (c). b) Detailed low energy SE image, 14 × 16 μm^2. c) VP SEM backscattered electron image with the same field of view. Note: lighter grayscale areas represent compressed aerogel.

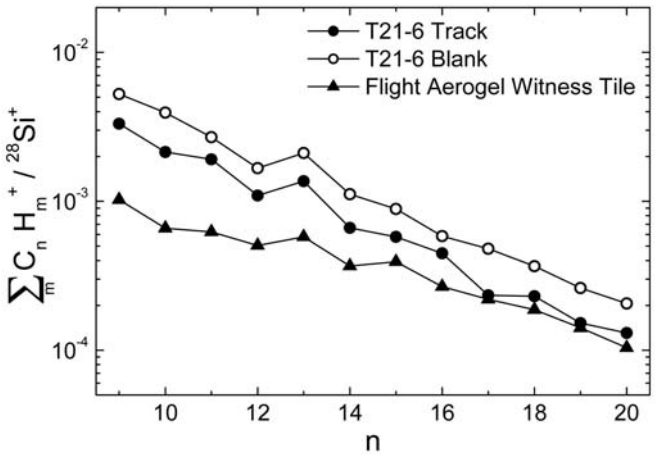

Fig. 12. Relative abundances of PAH secondary ions relative to the $^{28}Si^+$ signal depending on the number *n* of C atoms are shown for aerogel sample T21-6 directly at the track position and in the surrounding aerogel (blank). For comparison, results from the Flight Aerogel Witness Tile are shown. Relative statistical uncertainties of these measurements are between 2 and 23% for T21-6 and between 1 and 5% for the witness tile.

CONCLUSIONS

One of the major goals of the examination of Stardust samples is to reveal the bulk chemical composition of Wild 2. While the analysis of single grains often yields highly variable results, averaging large numbers of analyses yielded compositions that seem to be close to solar system abundances, represented by CI values (Flynn et al. 2006; Leitner et al. 2008; Stephan et al. 2008).

In the present study, both samples from Track 21 seem to represent such a large number of individual grains. Since individual particles were not recognized on the scale of observation of field emission VP SEM, the cometary matter in these samples seems to be nanometer-scale in dimension. Although only an exceedingly minute amount of the impacting particle was analyzed, this material provided enough substance that a strong correlation with chondritic composition was obtained.

From the close match of most observed element ratios with the solar system average, except for a depletion in Ca and an enrichment in Ni, it can be inferred that the fine-grained material in comet Wild 2 roughly represents average solar system material. Compared by mass, this ultrafine-grained cometary matter seems to be more representative of the composition of Wild 2 as a whole than is the coarser material, i.e., terminal particles and larger fragments. Concerning the missing Ca, this element is possibly concentrated in much larger mineral grains, probably CAI-like matter. The Ni enrichment, on the other hand, might be balanced by a depletion of Ni in some of the larger Wild 2 minerals, possibly Ni-poor iron sulfides.

The properties of Track 21, if characteristic for most Stardust tracks as indicated in Hörz et al. (2006), suggest that typical cometary particles consist of an intimate mixture of highly volatile matter containing organics, ultrafine minerals, and some coarser grains. During Stardust collection, while penetrating the aerogel, the ice vaporized explosively, distributing the ultrafine material in the walls of the emerging track bulbs. Some coarser, probably more robust grains survived this energetic disruption and were found as terminal particles or larger fragments.

Acknowledgments–This work was supported in part by the Deutsche Forschungsgemeinschaft through grant STE 576/17-1 and by the NASA Astrobiology Institute. The manuscript benefited from thorough reviews by David S. McPhail, Conel M. O'D. Alexander, and the associate editor Ian Lyon. The Stardust mission to comet 81P/Wild 2 was sponsored by NASA and executed jointly by the Jet Propulsion Laboratory and Lockheed Martin Space Systems. We are greatly indebted to many individuals who assured a successful comet encounter and who safely returned the Stardust collectors and their precious samples to Earth.

Editorial Handling—Dr. Ian Lyon

REFERENCES

Anders E. and Grevesse N. 1989. Abundances of the elements: Meteoritic and solar. *Geochimica et Cosmochimica Acta* 53:197–214.

Arndt P., Bohsung J., Maetz M., and Jessberger E. K. 1996. The elemental abundances in interplanetary dust particles. *Meteoritics & Planetary Science* 31:817–833.

Bajt S., Sandford S. A., Flynn G. J., Matrajt G., Snead C. J., Westphal A. J., and Bradley J. Forthcoming. Infrared spectroscopy of Wild 2 particle hypervelocity tracks in Stardust aerogel: Evidence for the presence of volatile organics in comet dust. *Meteoritics & Planetary Science.*

Brownlee D. E., Tsou P., Anderson J. D., Hanner M. S., Newburn R. L., Sekanina Z., Clark B. C., Hörz F., Zolensky M. E., Kissel J., McDonnell J. A. M., Sandford S. A., and Tuzzolino A. J. 2003. Stardust: Comet and interstellar dust sample return mission. *Journal of Geophysical Research* 108:E8111.

Brownlee D., Tsou P., Aléon J., Alexander C. M. O'D., Araki T., Bajt S., Baratta G. A., Bastien R., Bland P., Bleuet P., Borg J., Bradley J. P., Brearley A., Brenker F., Brennan S., Bridges J. C., Browning N. D., Brucato J. R., Bullock E., Burchell M. J., Busemann H., Butterworth A., Chaussidon M., Cheuvront A., Chi M., Cintala M. J., Clark B. C., Clemett S. J., Cody G., Colangeli L., Cooper G., Cordier P., Daghlian C., Dai Z., D'Hendecourt L., Djouadi Z., Dominguez G., Duxbury T., Dworkin J. P., Ebel D. S., Economou T. E., Fakra S., Fairey S. A. J., Fallon S., Ferrini G., Ferroir T., Fleckenstein H., Floss C., Flynn G., Franchi I. A., Fries M., Gainsforth Z., Gallien J.-P., Genge M., Gilles M. K., Gillet Ph., Gilmour J., Glavin D. P., Gounelle M., Grady M. M., Graham G. A., Grant P. G., Green S. F., Grossemy F., Grossman L., Grossman J. N., Guan Y., Hagiya K., Harvey R., Heck P., Herzog G. F., Hoppe P., Hörz F., Huth J., Hutcheon I. D., Ignatyev K., Ishii H., Ito M., Jacob D., Jacobsen C., Jacobsen S., Jones S., Joswiak D., Jurewicz A., Kearsley A. T., Keller L. P., Khodja H., Kilcoyne A. L. D., Kissel J., Krot A., Langenhorst F., Lanzirotti A., Le L., Leshin L. A., Leitner J., Lemelle L., Leroux H., Liu M.-C., Luening K., Lyon I., MacPherson G., Marcus M. A., Marhas K., Marty B., Matrajt G., McKeegan K., Meibom A., Mennella V., Messenger K., Messenger S., Mikouchi T., Mostefaoui S., Nakamura T., Nakano T., Newville M., Nittler L. R., Ohnishi I., Ohsumi K., Okudaira K., Papanastassiou D. A., Palma R., Palumbo M. E., Pepin R. O., Perkins D., Perronnet M., Pianetta P., Rao W., Rietmeijer F. J. M., Robert F., Rost D., Rotundi A., Ryan R., Sandford S. A., Schwandt C. S., See T. H., Schlutter D., Sheffield-Parker J., Simionovici A., Simon S., Sitnitsky I., Snead C. J., Spencer M. K., Stadermann F. J., Steele A., Stephan T., Stroud R., Susini J., Sutton S. R., Suzuki Y., Taheri M., Taylor S., Teslich N., Tomeoka K., Tomioka N., Toppani A., Trigo-Rodríguez J. M., Troadec D., Tsuchiyama A., Tuzzolino A. J., Tyliszczak T., Uesugi K., Velbel M., Vellenga J., Vicenzi E., Vincze L., Warren J., Weber I., Weisberg M., Westphal A. J., Wirick S., Wooden D., Wopenka B., Wozniakiewicz P., Wright I., Yabuta H., Yano H., Young E. D., Zare R. N., Zega T., Ziegler K., Zimmermann L., Zinner E., and Zolensky M. 2006. Comet 81P/Wild 2 under a microscope. *Science* 314:1711–1716.

Flynn G. J., Bleuet P., Borg J., Bradley J. P., Brenker F. E., Brennan S., Bridges J., Brownlee D. E., Bullock E. S., Burghammer M., Clark B. C., Dai Z. R., Daghlian C. P., Djouadi Z., Fakra S., Ferroir T., Floss C., Franchi I. A., Gainsforth Z., Gallien J.-P., Gillet Ph., Grant P. G., Graham G. A., Green S. F., Grossemy F., Heck P. R., Herzog G. F., Hoppe P., Hörz F., Huth J., Ignatyev K., Ishii H. A., Janssens K., Joswiak D., Kearsley A. T., Khodja H., Lanzirotti A., Leitner J., Lemelle L., Leroux H., Luening K., MacPherson G. J., Marhas K. K., Marcus M. A., Matrajt G., Nakamura T., Nakamura-Messenger K., Nakano T., Newville M., Papanastassiou D. A., Pianetta P., Rao W., Riekel C., Rietmeijer F. J. M., Rost D., Schwandt C. S., See T. H., Sheffield-Parker J., Simionovici A., Sitnitsky I., Snead C. J., Stadermann F. J., Stephan T., Stroud R. M., Susini J., Suzuki Y., Sutton S. R., Taylor S., Teslich N., Troadec D., Tsou P., Tsuchiyama A., Uesugi K., Vekemans B., Vicenzi E. P., Vincze L., Westphal A. J., Wozniakiewicz P., Zinner E., and Zolensky M. E. 2006. Elemental compositions of comet 81P/Wild 2 samples collected by Stardust. *Science* 314:1731–1735.

Hörz F., Bastien R., Borg J., Bradley J. P., Bridges J. C., Brownlee D. E., Burchell M. J., Chi M., Cintala M. J., Dai Z. R., Djouadi Z., Dominguez G., Economou T. E., Fairey S. A. J., Floss C., Franchi I. A., Graham G. A., Green S. F., Heck P., Hoppe P., Huth J., Ishii H., Kearsley A. T., Kissel J., Leitner J., Leroux H., Marhas K., Messenger K., Schwandt C. S., See T. H., Snead C., Stadermann F. J., Stephan T., Stroud R., Teslich N., Trigo-Rodríguez J. M., Tuzzolino A. J., Troadec D., Tsou P., Warren J., Westphal A., Wozniakiewicz P., Wright I., and Zinner E. 2006. Impact features on Stardust: Implications for comet 81P/Wild 2 dust. *Science* 314:1716–1719.

Leitner J., Stephan T., Kearsley A. T., Hörz F., Flynn G. J., and Sandford S. A. 2008. TOF-SIMS analysis of crater residues from Wild 2 cometary particles on Stardust aluminum foil. *Meteoritics & Planetary Science* 43. This issue.

Lodders K. and Fegley B. Jr. 1998. *The planetary scientist's companion*. New York: Oxford University Press. 371 p.

Sandford S. A., Aléon J., Alexander C. M. O'D., Araki T., Bajt S., Baratta G. A., Borg J., Bradley J. P., Brownlee D. E., Brucato J. R., Burchell M. J., Busemann H., Butterworth A., Clemett S. J., Cody G., Colangeli L., Cooper G., d'Hendecourt L., Djouadi Z., Dworkin J. P., Ferrini G., Fleckenstein H., Flynn G. J., Franchi I. A., Fries M., Gilles M. K., Glavin D. P., Gounelle M., Grossemy F., Jacobsen C., Keller L. P., Kilcoyne A. L. D., Leitner J., Matrajt G., Meibom A., Mennella V., Mostefaoui S., Nittler L. R., Palumbo M. E., Papanastassiou D. A., Robert F., Rotundi A., Snead C. J., Spencer M. K., Stadermann F. J., Steele A., Stephan T., Tsou P., Tyliszczak T., Westphal A. J., Wirick S., Wopenka B., Yabuta H., Zare R. N., and Zolensky M. E. 2006. Organics captured from comet 81P/Wild 2 by the Stardust spacecraft. *Science* 314:1720–1724.

Schramm L. S., Brownlee D. E., and Wheelock M. M. 1989. Major element composition of stratospheric micrometeorites. *Meteoritics* 24:99–112.

Stephan T. 2001. TOF-SIMS in cosmochemistry. *Planetary and Space Science* 49:859–906.

Stephan T., Butterworth A. L., Hörz F., Snead C. J., and Westphal A. J. 2006a. TOF-SIMS analysis of Allende projectiles shot into silica aerogel. *Meteoritics & Planetary Science* 41:211–216.

Stephan T., Butterworth A. L., Snead C. J., Srama R., and Westphal A. J. 2006b. TOF-SIMS analysis of aerogel picokeystones—An analogue to Stardust's interstellar dust collection (abstract #1448). 37th Lunar and Planetary Science Conference. CD-ROM.

Stephan T., Flynn G. J., Sandford S. A., and Zolensky M. E. 2008. TOF-SIMS analysis of cometary particles extracted from Stardust aerogel. *Meteoritics & Planetary Science* 43. This issue.

Tsou P., Brownlee D. E., Sandford S. A., Hörz F., and Zolensky M. E. 2003. Wild 2 and interstellar sample collection and Earth return. *Journal of Geophysical Research* 108:E8113.

Westphal A. J., Snead C., Butterworth A., Graham G. A., Bradley J. P., Bajt S., Grant P. G., Bench G., Brennan S., and Pianetta P. 2004. Aerogel keystones: Extraction of complete hypervelocity impact events from aerogel collectors. *Meteoritics & Planetary Science* 39:1375–1386.

Zolensky M. E., Zega T. J., Yano H., Wirick S., Westphal A. J., Weisberg M. K., Weber I., Warren J. L., Velbel M. A., Tsuchiyama A., Tsou P., Toppani A., Tomioka N., Tomeoka K., Teslich N., Taheri M., Susini J., Stroud R., Stephan T., Stadermann F. J., Snead C. J., Simon S. B., Simionovici A., See T. H., Robert F., Rietmeijer F. J. M., Rao W., Perronnet M. C., Papanastassiou D. A., Okudaira K., Ohsumi K., Ohnishi I., Nakamura-Messenger K., Nakamura T., Mostefaoui S., Mikouchi T., Meibom A., Matrajt G., Marcus M. A., Leroux H., Lemelle L., Le L., Lanzirotti A., Langenhorst F., Krot A. N., Keller L. P., Kearsley A. T., Joswiak D., Jacob D., Ishii H., Harvey R., Hagiya K., Grossman L., Grossman J. N., Graham G. A., Gounelle M., Gillet Ph., Genge M. J., Flynn G., Ferroir T., Fallon S., Ebel D. S., Dai Z. R., Cordier P., Clark B., Chi M., Butterworth A. L., Brownlee D. E., Bridges J. C., Brennan S., Brearley A., Bradley J. P., Bleuet P., Bland P. A., and Bastien R. 2006. Mineralogy and petrology of comet 81P/Wild 2 nucleus samples. *Science* 314:1735–1739.

APPENDIX

The following tables show for all analyzed samples secondary ion ratios prior to blank correction (raw data), the subtracted secondary ion signals for the aerogel blank, as well as the blank-corrected and renormalized ion ratios and the resulting atomic element ratios.

Data shown in italics were discarded for further evaluation, either because the blank signal was found to be higher than 50% of the entire signal, or because these elements show a rather heterogeneous distribution in the aerogel blank.

Statistical 1σ errors are given as last significant digit in parentheses.

Table A1. TOF-SIMS data for sample T57 particle #1.

	Raw data	Blank	Corrected data	
Element	(ions/Fe^+)	(ions/Fe^+_{raw})	(ions/Fe^+)	(elem./Fe)
Li	0.08(1)	0.003(3)	0.09(1)	0.017(2)
B	0.43(2)	0.03(1)	0.46(3)	1.44(9)
Na	1503(1)	8.1(1)	1732(2)	187.0(2)
Mg	154.5(5)	0.04(1)	179.0(6)	54.9(2)
Al	170.1(7)	0.13(3)	197.0(8)	64.4(3)
Si[a]	*2257(7)*	*2239(7)*	*20(10)*	*50(30)*
K	1156(1)	4.6(1)	1334(2)	85.6(1)
Ca	130.5(6)	0.006(8)	151.2(7)	26.1(1)
Sc	*0.010(3)*	*0.00(2)*	*0.01(2)*	*0.003(9)*
Ti	1.4(2)	0.01(1)	1.6(2)	0.65(8)
V	*0.015(4)*	*0.03(1)*	*–0.01(2)*	*–0.006(7)*
Cr	0.054(8)		0.06(1)	0.029(4)
Mn	*0.021(5)*	*0.02(4)*	*0.00(5)*	*0.00(3)*
Fe	1.00(3)	0.14(2)	1.00(5)	1.00(5)
Co	*0.000(1)*		*0.000(1)*	*0.001(2)*
Ni	0.016(6)	0.00(1)	0.02(1)	0.04(3)
Cu	*0.07(1)*	*0.04(1)*	*0.03(2)*	*0.08(6)*
Ba	0.23(2)		0.27(2)	0.055(4)

[a]A CI chondritic Si/Mg ratio was assumed during blank correction because the sample is rather Fe-poor.

Table A2. TOF-SIMS data for sample T57 particle #2

	Raw data	Blank	Corrected data	
Element	(ions/Fe^+)	(ions/Fe^+_{raw})	(ions/Fe^+)	(elem./Fe)
B	*0.00008(6)*	*0.000019(6)*	*0.00006(6)*	*0.0002(2)*
Na	0.252(3)	0.00488(8)	0.247(3)	0.0267(3)
Mg	0.0138(8)	0.000027(7)	0.0138(8)	0.0042(2)
Al	*0.00012(7)*	*0.00008(2)*	*0.00004(7)*	*0.00001(2)*
Si[a]	1.345(8)	1.343(4)	0.002(9)	0.00(2)
K	0.042(1)	0.00273(7)	0.040(1)	0.00255(8)
Ca	0.0009(2)	0.000003(5)	0.0009(2)	0.00015(3)
Cr	*0.00008(6)*		*0.00008(6)*	*0.00003(3)*
Mn	*0.0002(1)*	*0.00001(3)*	*0.0002(1)*	*0.00009(6)*
Fe	1.000(8)	0.00008(1)	1.000(8)	1.000(8)
Co	*0.00014(8)*		*0.00014(8)*	*0.0002(1)*
Ni	0.0016(5)	0.000001(6)	0.0016(5)	0.004(1)

[a]A CI chondritic Si/Mg ratio was assumed during blank correction because the sample is dominated by Fe sulfide.

Table A3. TOF-SIMS data for sample T57 particle #3

	Raw data	Blank	Corrected data	
Element	(ions/Fe^+)	(ions/Fe^+_{raw})	(ions/Fe^+)	(elem./Fe)
Li	0.05(2)	0.0001(1)	0.05(2)	0.010(3)
Na	52.7(5)	0.364(6)	52.6(5)	5.68(5)
Mg	28.0(4)	0.0020(5)	28.2(4)	8.7(1)
Al	3.3(1)	0.006(1)	3.3(1)	1.09(4)
Si[a]	*103.6(9)*	*100.2(3)*	*3.4(9)*	*8(2)*
K	4.3(1)	0.204(5)	4.1(1)	0.262(9)
Ca	4.3(1)	0.0003(4)	4.3(1)	0.75(2)
Sc	*0.004(4)*	*0.0002(9)*	*0.004(5)*	*0.002(2)*
Ti	0.15(3)	0.0005(5)	0.15(3)	0.06(1)
V	*0.009(6)*	*0.0011(6)*	*0.008(6)*	*0.004(3)*
Cr	0.51(5)		0.51(5)	0.23(2)
Mn	0.09(2)	0.001(2)	0.09(2)	0.05(1)
Fe	1.00(8)	0.006(1)	1.00(8)	1.00(8)
Co	*0.004(4)*		*0.004(4)*	*0.007(7)*
Ni	0.02(1)	0.0000(5)	0.02(1)	0.06(3)
Cu	*0.013(9)*	*0.0019(7)*	*0.011(9)*	*0.03(2)*
Ba	*0.005(6)*		*0.005(6)*	*0.001(1)*

[a]A CI chondritic Si/Mg ratio was assumed during blank correction because the sample is rather Fe-poor.

Table A4. TOF-SIMS data for sample T21-6

	Raw data	Blank	Corrected data	
Element	(ions/Fe^+)	(ions/Fe^+_{raw})	(ions/Fe^+)	(elem./Fe)
Li	*0.002(1)*	*0.002(1)*	*0.000(2)*	*0.0000(3)*
B	*0.096(9)*	*0.097(6)*	*0.00(1)*	*0.00(4)*
Na	1.37(3)	0.65(1)	0.74(4)	0.080(4)
Mg	2.02(4)	0.035(4)	2.04(4)	0.63(1)
Al	0.20(1)	0.005(3)	0.20(1)	0.065(4)
Si	*138.1(7)*	*137.6(6)*	*0.5(9)*	*1(2)*
K	*0.59(2)*	*0.43(1)*	*0.16(3)*	*0.011(2)*
Ca	0.089(8)	0.012(2)	0.079(9)	0.014(2)
Sc	*0.005(3)*	*0.003(2)*	*0.002(3)*	*0.001(1)*
Ti	*0.004(2)*	*0.004(1)*	*0.000(3)*	*0.000(1)*
Cr	0.028(5)	0.001(1)	0.028(6)	0.013(3)
Mn	0.017(8)	0.001(4)	0.02(1)	0.009(5)
Fe	1.00(3)	0.027(5)	1.00(3)	1.00(3)
Co	0.003(2)		0.003(2)	0.005(3)
Ni	0.054(9)		0.056(9)	0.14(2)

Table A5. TOF-SIMS data for sample T21-2.

	Raw data	Blank	Corrected data	
Element	(ions/Fe^+)	(ions/Fe^+_{raw})	(ions/Fe^+)	(elem./Fe)
Li	*0.003(2)*	*0.0023(2)*	*0.001(2)*	*0.0002(4)*
B	*0.19(2)*	*0.204(2)*	*–0.02(2)*	*–0.05(5)*
Na	*1.11(3)*	*0.896(4)*	*0.21(3)*	*0.023(4)*
Mg	3.38(7)	0.0374(9)	3.39(7)	1.04(2)
Al	0.37(2)	0.0040(3)	0.37(2)	0.120(7)
Si	*193.7(5)*	*193.23(6)*	*0.5(5)*	*1(1)*
K	*1.93(6)*	*0.878(5)*	*1.07(6)*	*0.069(4)*
Ca	0.08(1)	0.0025(3)	0.08(1)	0.013(2)
Ti	0.013(5)	0.0031(3)	0.010(5)	0.004(2)
Cr	0.033(6)	0.0013(2)	0.032(7)	0.014(3)
Mn	0.019(7)	0.0005(1)	0.019(7)	0.010(4)
Fe	1.00(4)	0.014(1)	1.00(4)	1.00(4)
Co	0.002(1)	0.00004(4)	0.002(1)	0.003(2)
Ni	0.077(9)	0.0010(2)	0.08(1)	0.19(2)

Table A6. TOF-SIMS data for sample T21-2 Detail #1.

	Raw data	Blank	Corrected data	
Element	(ions/Fe^+)	(ions/Fe^+_{raw})	(ions/Fe^+)	(elem./Fe)
Li	*0.0024(4)*	*0.0013(1)*	*0.0011(5)*	*0.00020(9)*
B	*0.119(3)*	*0.120(1)*	*–0.001(4)*	*0.00(1)*
Na	*0.957(9)*	*0.526(2)*	*0.435(9)*	*0.047(1)*
Mg	5.36(2)	0.0220(5)	5.38(2)	1.651(7)
Al	0.365(6)	0.0023(2)	0.366(6)	0.120(2)
Si	*113.9(1)*	*113.39(3)*	*0.5(1)*	*1.1(2)*
K	*0.484(6)*	*0.515(3)*	*–0.032(7)*	*–0.0020(5)*
Ca	0.113(5)	0.0015(2)	0.112(5)	0.0194(9)
Ti	0.008(1)	0.0018(2)	0.006(1)	0.0025(4)
Cr	0.032(2)	0.0008(1)	0.031(2)	0.0141(8)
Mn	0.035(2)	0.00028(6)	0.035(2)	0.019(1)
Fe	1.00(1)	0.0084(6)	1.00(2)	1.00(2)
Co	0.0019(4)	0.00003(3)	0.0019(4)	0.0029(6)
Ni	0.027(3)	0.0006(1)	0.027(3)	0.067(7)

Table A7. TOF-SIMS data for sample T21-2 Detail #2.

	Raw data	Blank	Corrected data	
Element	(ions/Fe^+)	(ions/Fe^+_{raw})	(ions/Fe^+)	(elem./Fe)
Li	*0.0015(3)*	*0.00084(7)*	*0.0007(3)*	*0.00013(6)*
B	*0.062(2)*	*0.0756(8)*	*–0.014(2)*	*–0.044(7)*
Na	0.752(6)	0.332(1)	0.422(7)	0.0456(7)
Mg	4.51(2)	0.0139(3)	4.52(2)	1.387(5)
Al	0.25(1)	0.0015(1)	0.25(1)	0.082(3)
Si	*72.16(6)*	*71.69(2)*	*0.47(7)*	*1.1(2)*
K	*0.507(5)*	*0.326(2)*	*0.182(6)*	*0.0117(4)*
Ca	0.182(4)	0.0009(1)	0.182(4)	0.0315(7)
Ti	0.0042(6)	0.0011(1)	0.0030(6)	0.0012(3)
Cr	0.039(2)	0.00048(6)	0.039(2)	0.0175(7)
Mn	0.023(2)	0.00018(4)	0.023(2)	0.0128(9)
Fe	1.00(1)	0.0053(4)	1.00(1)	1.00(1)
Co	0.0014(3)	0.00002(2)	0.0014(3)	0.0022(4)
Ni	0.038(3)	0.00036(7)	0.038(3)	0.095(7)